

Tropical Cyclone Simulation and Response to CO₂ Doubling in the GFDL CM2.5 High-Resolution Coupled Climate Model

Hyeong-Seog Kim^{1,2,3}, Gabriel A. Vecchi¹, Thomas R. Knutson¹, Whit G. Anderson¹, Thomas L. Delworth¹, Anthony Rosati¹, Fanrong Zeng¹, Ming Zhao^{1,4}

¹NOAA/Geophysical Fluid Dynamics Laboratory, Princeton, NJ

²Atmospheric and Oceanic Sciences, Princeton University, Princeton, NJ

³Willis Research Network, London, UK

⁴University Corporation for Atmospheric Research, Boulder, CO

J. Climate (to be submitted)

July 18, 2013

Abstract

Global tropical cyclone (TC) activity is simulated by the Geophysical Fluid Dynamics Laboratory (GFDL) CM2.5 model, which is a fully coupled global climate model with horizontal resolution of about 50km for atmosphere and 25 km for ocean. The present-day climate simulation shows fairly realistic global TC frequency, TC seasonal cycle, and geographical distribution in the various basins. The model has some notable biases in regional TC activity, including simulating too few TCs in the North Atlantic basin. The regional biases in TC activity are associated with simulation biases in the large-scale environment such as sea surface temperature, vertical wind shear, and 500 hPa vertical velocity. Despite these biases, the model simulates the large-scale variations of TC activity induced by El Nino/Southern Oscillation fairly realistically.

The response of TC activity in the model to global warming is investigated by comparing the present climate with a CO₂ doubling experiment. Globally, TC frequency decreases (-19%) while TC lifetime-maximum intensity increases (+2.7%) in response to the CO₂ doubling, consistent with previous studies. The average TC lifetime decreases by -4.6%, while the TC size and TC-induced rainfall rate increase by about 3% and 12%, respectively. These changes are generally reproduced across the different basins in terms of the sign of the change, although the percent changes vary from basin to basin and within individual basins. For the Atlantic basin, the reduced TC frequency in the CO₂ warmed climate occurs in association with decreased relative SST and increased vertical wind shear over the main development and surrounding regions. Although there is an overall reduction in frequency in the Atlantic from CO₂ doubling, the warmed climate exhibits increased interannual hurricane frequency variability so that the simulated Atlantic TC activity is enhanced more during unusually warm years in the CO₂-

44 warmed climate relative to that in unusually warm years in the control climate.

1. Introduction

Tropical cyclones (TC) are very destructive storms that can cause severe damage due to high winds, rainfall, and storm surge (Peilke et al. 2008, Mendelsohn et al. 2012). Thus, improved scientific understanding of TC behavior in the context of global climate change is an important issue for long-range planning and policy-makers.

There have been a number of previous studies simulating TCs using global climate models in order to examine the changes of TC frequency under global warming scenarios. The earliest such studies used models with relatively coarse resolutions, and typically without full ocean coupling (e.g., Broccoli and Manabe 1990; Haarsma et al. 1993; Bengtsson et al. 1996). As computing power has increased, these TC simulations have become more realistic, with Zhao et al. (2009) providing an example of the ability of current models to reproduce the interannual variability of Atlantic hurricane counts when forced by observed SST. A summary of the most recent generation of such TC-climate studies (Knutson et al. 2010) indicates a growing consensus among models of a reduction in global TC frequency in a warmer climate, with a projected decrease of 6-34 % by the end of the 21st century. The present study attempts to further build on these results using a new state-of-the-art high resolution coupled climate model.

Concerning TC intensity, global climate model simulations of TCs typically have not been able to simulate storms as intense as observed owing to their coarse resolution, although recent global model studies are progressing toward higher resolution and more realistic intensity distributions (e.g., Bengtsson et al. 2007; Murakami et al. 2012), albeit without ocean coupling. As a different approach, one way to address the limited resolution of global models has to use, regional dynamical or statistical/dynamical downscaling techniques (Knutson et al. 1998, Emanuel et al. 2008, Bender et al. 2010, Mendelsohn et al. 2012, Knutson et al. 2013). These downscaling

techniques use large-scale input from the global models and can provide more realistic distributions of TC intensities. Climate change experiments with these downscaling models, as well as the global model study of Murakami et al. (2012), suggest that the number of TCs that reach category 4–5 intensity could increase in the future. A recent assessment of TC intensity projection studies finds a 2–11% increase in response to projected 21st century warming (Knutson et al. 2010)

In this study, we analyze global TC activity and its response to climate warming as simulated by the Geophysical Fluid Dynamics Laboratory (GFDL) Climate Model version 2.5 (CM2.5) (Delworth et al. 2011). The CM2.5 is a coupled atmosphere-ocean-land-cryosphere model that differs from atmospheric GCMs running with prescribed SST by simulating the ocean-atmosphere interaction that is a crucial factor in development of TC. In comparison to other recent efforts using fully coupled models (Gualdi et al. 2008) the CM2.5 model uses a higher resolution atmosphere (~50 km grid) and is one of the highest resolution fully coupled GCMs in use today for such climate change studies.

The rest of this paper is organized as follows. The data for observed TCs and atmospheric and oceanic environments is introduced in the section 2. The model experiments using the GFDL CM2.5 are also briefly described in this section. Comparisons between observed and model-simulated climatological TC activity are presented in the section 3, and the simulated response to the CO₂ doubling is examined in section 4. Section 5 contains the discussion and conclusions.

2. Data & Method

a. Observational data

The observed TC data used in the study was obtained from the International Best Track Archive for Climate Stewardship (IBTrACS) data archived by the National Climate Data Center (Knapp et al. 2010). In this study, we use 6-hourly locations and intensity of TCs in the tropical storm and hurricane stages (i.e., sustained wind speed $> 17 \text{ m s}^{-1}$). We analyze only TCs observed during recent 30 years (1981-2010) to avoid reliability problems in the occurrence and intensity data for TCs during the period prior to satellite observation.

The National Center for Environmental Prediction-Department of Energy reanalysis version 2 (NCEP-DOE R2) (Kanamitsu et al. 2002) and NOAA Extended Reconstructed sea surface temperature version 3 (ERSSTv3) (Smith et al. 2008) are used to evaluate the model-simulated environments affecting TC activity. The data sets were obtained from the ftp site of the NOAA Climate Diagnosis Center; the horizontal resolutions are 2.5 degree for NCEP-DOE R2 and 2 degree for ERSSTv3. We do not use the atmospheric reanalysis for any trend analysis here for reasons discussed in Vecchi et al. (2013).

b. GFDL CM2.5

The GFDL CM2.5 is a newly developed high-resolution global climate model, with coupled atmosphere, ocean, land, and sea ice components (Delworth et al. 2011). The model is derived closely from the GFDL CM2.1 model (Delworth et al. 2006), which was one of the global models used in the Intergovernmental Panel on Climate Change (IPCC) Fourth Assessment Report (AR4). The atmospheric component of CM2.5 uses a finite volume dynamical core formulated on a cubed-sphere grid (Lin 2004; Putman and Lin 2007) that allows roughly equal-area grid boxes over the globe. The atmospheric model has a horizontal grid-spacing of approximately 50 km and a vertical resolution of 32 levels. This model uses the relaxed

Arakawa-Schubert convection scheme (Moorthi and Suarez 1992) and the K-profile convective boundary layer scheme (Lock et al. 2000). The ocean component is based on the Modular Ocean Model version 4.1 (Griffies 2010) and has a horizontal grid-spacing of roughly 25 km (from 28 km at the equator to 8~11 km at high-latitude) with 50 vertical levels. For the land and sea ice components, the GFDL LM3 and Sea Ice Simulator are used, respectively. The simulated climate in CM2.5 showed significant improvement over the tropics compared to CM2.1, including a reduction in biases in the seasonal variation of the intertropical convergence zone (ITCZ) as well as an improved simulation of some aspects of the El Nino/Southern Oscillation (ENSO) and its teleconnections (Delworth et al. 2012). In addition, CM2.5 simulates a relatively realistic regional rainfall over the Amazon, Sahel, and Indian Monsoon regions and climate over the tropical north Atlantic (Delworth et al. 2012, Doi et al. 2012).

In this study, we use two CM2.5 experiments:

- Control: Present climate experiment. A 280-year simulation with constant 1990 levels of various climate forcing agents.
- 2×CO₂: CO₂ doubling experiment. A 140-year simulation, spun off from year 101 of the control simulation, but with a 1% yr⁻¹ increase in atmospheric CO₂ concentration for years 1-70 (until CO₂ reaches twice its initial value) and then constant (2x) CO₂ concentration for years 71-140.

We conduct an analysis only for years 91–140 for both experiments to focus on the approximately steady state response to CO₂ doubling (Doi et al. 2013).

The TC detection and tracking algorithm used in this study is same as that described in Zhao et al. (2009). The algorithm selects warm-core vortices that satisfy the certain criteria in the 6-

135 hourly model outputs and connects them into individual TC tracks. The criteria used in this study
136 are as follows:

- 137 • The 850-hPa relative vorticity maxima higher than $3.5 \times 10^{-5} \text{ s}^{-1}$ are located within a $6^\circ \times 6^\circ$
138 latitude-longitude area.
- 139 • The local minimum of sea level pressure, which must be within 2° of the vorticity
140 maximum is defined as the storm center.
- 141 • The local maximum of temperature averaged between 300 and 500 hPa (warm core
142 center) must be within 2° of the local minima of sea level pressure and the warm core
143 temperature must be at least 1 K warmer than the surrounding local mean.
- 144 • The initial point of the storm trajectory must be between 40°S and 40°N and the distance
145 between two “connected” vortex locations must be less than 400 km in 6 hours.
- 146 • The trajectory must last at least 3 days (not necessarily consecutive) with maximum
147 winds exceeding 17 m/s.

148 The TC maximum wind speed is obtained using the lowest level of the atmospheric model (35
149 m). This wind speed is about 10% larger than the 10-m wind speed that is used for TC intensity
150 in observed TC data sets (Zhao et al. 2012). Thus, using the wind speed at the lowest model level
151 is roughly equivalent to applying a 10% lower intensity criterion on simulated tropical storms
152 than is applied to observed storms. Walsh et al. (2007) suggest that resolution-dependent criteria
153 for sustained TC wind speeds be used in model simulation analyses to reflect the effect of the
154 coarse horizontal resolutions on the intensity of the modeled storms. The 10 % reduction in wind
155 speed criterion we use is in the range recommended by Walsh et al. for a 50-km grid model.

156

3. Present Day Cyclone Simulation

a. TC climatology

Figure 1 shows the geographical distribution of TC tracks in observations and the CM2.5 control simulation. For convenience of analysis, the global TC activity is divided into seven basins, i.e., North Atlantic (NA), East Pacific (EP), West Pacific (WP), North Indian Ocean (NI), South Indian Ocean (SI) and South Pacific (SP) as denoted in Fig. 1a. The boundaries of the basins are used in IBTrACS. In observations, TCs form over most of the tropical oceans except for the southeastern Pacific and South Atlantic which have relatively cool sea surface temperatures and strong vertical wind shear. The CM2.5 simulates the general observed geographical characteristics of TC tracks over the globe (Fig. 1). The observed and simulated annual TC counts in each of the basins are compared in Fig. 2. Although the global TC count simulated in CM2.5 (82.0 yr^{-1}) shows quite good agreement with observations (82.4 yr^{-1}), there are substantial biases in TC counts in some basins (Fig. 2). In particular, the number of simulated TCs in the North Atlantic is only about one-quarter of that in observation (11.4 yr^{-1} in IBTrACS vs. 2.7 yr^{-1} in CM2.5). Several basins have the TC counts comparable to the observations (16.1 yr^{-1} in observation vs. 16.6 yr^{-1} in CM2.5 for EP, 26.1 vs. 27.5 yr^{-1} for WP, and 4.0 vs. 5.5 yr^{-1} for NI).

Examining the simulated TCs over the NA in more detail, (Fig. 1b), most of the model TCs there are formed over the vicinity of the main development region (MDR; 80°W - 20°W , 10°N - 20°N , Goldenberg and Shapiro 1996); TC formation is especially deficient over the Gulf of Mexico and east of Florida. Meanwhile, in the central North Pacific (170° - 150°W) and Arabian Sea (west of 75°E) CM2.5 simulates more TC activity than observed (Chu 2002, Evan and Camargo 2011), contributing to slightly positive biases in the simulated TC activity over the North Pacific

and North Indian Ocean as a whole. In the Southern Hemisphere, the CM2.5 produces more TCs than observed over the South Indian Ocean (16.0 yr^{-1} in observation vs. 21.7 yr^{-1} in CM2.5) and fewer than observed in the South Pacific (10.9 yr^{-1} in observation vs. 7.8 yr^{-1} in CM2.5).

As a sensitivity test, we used a weaker criteria on TC detection (e.g., 12 m s^{-1} for wind speed, 0.75 K for warm core and/or 2 days for duration) to see its effect on the TC count in the NA. The results show that even if we applied weaker criteria, a substantial negative bias over the North Atlantic remains. It indicates that the CM2.5 simulation has systematic biases that suppress TC activity in this vicinity, as will be discussed later.

Figure 3 presents the seasonal cycle of observed and simulated TCs in each of the basins. The model shows a fairly realistic seasonal cycle of TC counts, with a peak during the summer season of each hemisphere except for the Northern Indian Ocean. For the Northern Indian Ocean, the observed seasonal cycle of TCs has a bimodal shape with peaks in both spring and fall, as the TC activity in this basin is suppressed by strong vertical wind shear during the summer monsoon season. The CM2.5 captures only one of these peaks (the post monsoon season). Although the number of TCs over the North Atlantic in CM2.5 is smaller than the observation for all months, its annual cycle is captured well (Fig. 3a). For the other basins, the positive bias in the monthly number of TC formation tends to be found in the mid and late TC seasons rather than early season.

To investigate the environmental factors affecting the aforementioned characteristics of the TC activity in CM2.5, the SST, vertical wind shear, and 500-hPa vertical pressure velocity ($\omega_{500\text{hPa}}$) are analyzed as potential contributing factors (Fig. 4). The vertical wind shear is computed as the amplitude of the difference vector between winds at 200 and 850 hPa. Figure 4 shows the model bias in these fields during boreal summer (July–October) for the Northern Hemisphere

and austral summer (December–March) for the Southern Hemisphere. During the boreal summer, the SST simulated in CM2.5 has cold bias in the North Atlantic and much of the subtropical western and central North Pacific. The model has a warm bias in the eastern North Pacific and much of the North Indian Ocean (Fig. 4a). Although the SST bias is smaller in CM2.5 than in the CM2.0 and CM2.1 coupled models, significant biases remain as discussed by Doi et al. 2012. Along with the cold SST bias in the North Atlantic, CM2.5 simulates stronger vertical wind shear and reduced upward flow over the tropical and subtropical North Atlantic during boreal summer (Fig. 4b–c). The warm bias in eastern Pacific and cold bias in the North Atlantic in CM2.5 may lead to the strong vertical wind shear bias and anomalous descent over the NA basin, analogous to ENSO affects on the Atlantic region (Goldenberg and Shapiro 1996, Vecchi and Soden 2007). These model biases would all act to inhibit CM2.5 from producing TCs over the North Atlantic. Meanwhile, CM2.5 has a negative bias in the vertical wind shear and 500-hPa omega (i.e., anomalous rising motion) over the central and eastern tropical North Pacific and the Arabian Sea (Fig. 4a–c), which would be expected to lead to more vigorous TC activity in these regions. For the Southern Hemisphere, CM2.5 simulates vertical wind shear that is generally too strong, anomalous sinking motions and a cold SST bias over the tropics and subtropics in the South Pacific during austral summer (Fig. 4d–f). Although these factors would act to suppress TC formation in the southern hemisphere, there does not appear to be an overall bias in TC frequency in the Southern Hemisphere-

TC activity over the NA basin is known to have a strong statistical relationship with the vertical wind shear over the MDR (e.g., Goldenberg and Shapiro 1996; Landsea et al 1998; Wang et al. 2009). Figure 5 illustrates the relationship between the vertical wind shear and the Atlantic tropical storms during August-October in both observations and CM2.5. The MDR

vertical wind shear and Atlantic TC counts are negatively correlated in observations ($r=-0.60$) as well as the CM2.5 control ($r=-0.41$) and $2\times\text{CO}_2$ ($r=-0.42$) experiments. The MDR vertical wind shears in CM2.5 simulations are much higher than those in the observation (Fig. 5). The Atlantic TC activity would apparently be suppressed even in observations if the magnitude of the vertical wind shear were as strong as in CM2.5. Interestingly, the overall bias in shear and NA TC frequency in this model is consistent with an extrapolation of the observed shear/TC relationship.

In summary, we conclude that the significant negative bias of TCs in the NA basin is likely largely a response of the CM2.5 model to biases in its simulated large-scale climatology (e.g., SST and vertical wind shear). This further suggests that the simulation skill for TC activity in the model could be improved if the model biases in climatological SST and wind shear were reduced.

b. Interannual variability: ENSO-related variation

To explore the simulation of the interannual variability of TC activity in CM2.5, we focus on the relationship between the model's TC activity and ENSO, since ENSO is known to be a key phenomenon affecting the interannual variation of TC activity over the global tropics (e.g., Wang and Chan 2002, Camargo and Sobel 2005, Kuleshov et al. 2008, Klotzbach 2011). Figure 6 shows a map of TC occurrences regressed on the seasonal mean NINO3.4 index. Here, the TC occurrence is defined as the number of TC days accumulated over the summer season: June to October for the Northern Hemisphere (Fig. 6a-b) and December to March for the Southern Hemisphere (Fig. 6c-d). We used 6-hourly TC track information obtained from the IBTrACS and the CM2.5 simulation. These simultaneous (unlagged) regression results for the NINO3.4 index reproduce well-known ENSO-dependent TC variations in both hemispheres (Fig. 6a, c).

During El Nino, the boreal summer TC activity increases in the southeastern part of the western North Pacific and central/eastern North Pacific, and decreases in the northwestern part of the western North Pacific and North Atlantic, with opposite changes during La Nina. For the Southern Hemisphere, enhanced TC activity is observed during El Nino over the South Pacific while the TC activity is reduced in the northwestern offshore of Australia, again with opposite change during La Nina (Fig. 6c). As shown in Fig. 6b and 5d, the CM2.5 simulations show good agreement with key features of the observed ENSO signal in the TC activity, such as the eastward shift of TCs in the western North Pacific (Fig. 6b) and enhancement of TC activity in the South Pacific (Fig. 6d). The negative relationship between El Nino and North Atlantic TC activity is also captured in CM2.5 despite the negative biases in climatological Atlantic TC frequency. The variation of TC activity related to ENSO in the observation has been related to changes in the vertical wind shear and relative vorticity forced by the zonal gradient of tropical SST anomalies associated with ENSO (Wang and Chan 2002, Camargo et al. 2007). CM2.5 has a marked improvement in the simulation of ENSO and its related large-scale circulation anomalies compared to earlier GFDL models such as CM2.1 (Delworth et al. 2012) and this likely helps with the successful simulation of ENSO-related TC activity changes. Overall, our analysis suggests that CM2.5 has sufficient realism to be useful for exploring the TC response to the changes in the large-scale environments, such as could occur with climate warming.

4. Changes in TC activity in response to CO₂ doubling

The response of TC activity in CM2.5 to a CO₂ doubling is investigated in this section. As shown in Table 1, CM2.5 simulates a significant reduction of TC genesis in response to CO₂ doubling, which is consistent with a number of previous studies (e.g., Knutson et al. 2010). A

significant reduction simulated is in each of the six individual basins (Table 1). The magnitude of these changes (-19 % for the globe with ranges from -13 % in the North Indian Ocean to -28 % in the North Atlantic), are in general agreement with values from previous studies (Bengtsson et al. 2007, Knutson et al. 2010, Murakami et al. 2011, Held and Zhao 2011), yet most of these studies showed regions of increase and decrease in contrast with the ubiquitous decrease seen here. The global number of TCs developing to hurricane strength also decreases significantly ($p < 0.05$) (-9.2 %). The fractional decrease, however, is smaller than for all TCs and a consistent signal is not seen across all basins, with only the South Indian Ocean decrease being significant. The fraction of TCs that reach hurricane intensity increases in most basins with the largest increases simulated in the North Hemisphere basins. These results indicate the model simulated TCs are intensified in the 2xCO₂ climate, although their frequency are reduced, which is consistent with previous studies (*e.g.*, Knutson et al. 2010).

Figure 7 shows box-whisker plots that illustrate statistical distributions of the lifetime-maximum wind speeds and lifetimes of TCs simulated in CM2.5 control and 2xCO₂ experiments. In terms of global statistics, the maximum wind speed increases systematically in the 2xCO₂ simulation for all percentiles examined (*i.e.*, 1st, 25th, 50th, 75th and 99th percentiles). It is noted that this model cannot simulate very intense TCs (*e.g.*, none are simulated that have lowest model level wind speed of more than 50 m/s, which is the Saffir-Simpson surface wind speed threshold for major hurricanes (categories 3–5). This is a qualitatively similar limitation of TC simulations to that using other dynamical models with similar horizontal resolutions (*e.g.*, Zhao et al. 2009). The percent change in the mean of the global TC maximum wind speed distribution is 2.7 %. The difference between the two global distributions in Fig. 7 is statistically significant ($p < 0.01$) using a two-sided Mann-Whitney U-

test. The increase of mean TC maximum wind speed is statistically significant in the Northern Hemisphere basins (2.7–4.3%) while it is smaller and not significant in the Southern Hemisphere basins (1.2–1.5%) (Table 2; Fig. 7). It is also notable that the box-whisker plots show a larger increase in the highest percentile of TC wind speed than the percentiles including the median, suggesting an enhanced climate change signal for the stronger storms, reminiscent of that found in some observational studies of intensity (e.g., Elsner et al. 2008). Despite the model's limitation in simulating intense TCs, we can cautiously infer an increase of stronger TCs in the warmed climate from our results. Our global TC intensity change results seem generally consistent with projections from other recent studies using dynamical downscaling methods, although those also used different future climate forcing scenarios. For example, Bender et al. 2010, Knutson et al. 2013, show a fairly robust enhancement in the frequency of very intense TCs in category 4–5 in their model future, although this change was smaller for CMIP5 RCP4.5 multi-model projections than for CMIP3 A1B multi-model projections. It is worth notifying that the CMIP5 forcing sources include change to non-greenhouse gases, while the present study focuses solely on the role of CO₂.

The simulated TC lifetimes (Table 2, Fig. 7) become shorter on average in the 2×CO₂ simulation. Because of the lifetime criterion in the TC detection algorithm used in this study, there is little change in the lowest bounds for lifetime. The changes, however, become larger at the upper percentiles. The change in the global TC lifetime distribution is statistically significant ($p < 0.01$), with a change in the mean of -5.2 %. Similar reductions are also found over most of the individual basins although the significant changes are found only in the western North Pacific and South Indian Ocean (Fig. 7, Table 2). It is noted that this decrease in the TC lifetimes is not

consistent with the results of Bengtsson et al. (2007) who found a minor increase in the lifetimes of TCs in their climate warming experiments.

We also have examined the TC traveling distance (track length) and found that this decreases globally, and the percent changes in each of the individual basins tend to mirror the changes in TC lifetime (Table 2) in terms of magnitude and statistical significance. The translation speed of TCs shows no significant changes between the control and $2\times\text{CO}_2$ experiments, which is consistent with the results of a recent downscaling study for the Atlantic basin only, using the CMIP5 models (Knutson et al. 2013). The translation speed of TCs is one of the major factors influencing the potential damage from TCs because slow-moving TCs have a greater possibility to afflict a larger area with a longer duration of strong winds (Mahendran 1998; Holland et al. 2010). Our results suggest that the contribution of translation speed changes to potential damage changes from TCs may be minor in this type of warmed climate scenario.

The TC size is also recognized as an important parameter influencing TC damage potential because it roughly controls the width of the “damage swath” induced by strong wind gusts of landfalling TCs (Powell and Reinhold 2007, Maclay et al. 2008) and can also contribute to the magnitude and areal extent of the storm surge, as illustrated by US hurricanes Isabel (2003), Katrina (2005), and Sandy (2012). In this study, we examine the TC size using the mean radius of 12 m/s (R12), 15m /s (R15) and 25 m/s (R25) azimuthally averaged tangential wind speeds. This wind speed metric is used in our calculation of TC size to reduce the influence of the background wind. Figure 8 shows the mean TC size for each basin in the Control and $2\times\text{CO}_2$ experiments. For comparison with the observation, we use the R12 estimated from the QuikSCAT surface wind (Chavas and Emanuel, 2010) for all basins and R15 and R25 retrieved from aircraft data for the western North Pacific by Weatherford and Gray (1988). Overall, the

340 Control run simulated TC sizes are systematically larger than those estimated from observations.
341 This could be due to the limited horizontal resolution (~50 km grid) of CM2.5 limiting the
342 model's ability to simulate small size TCs. In terms of the interbasin differences in TC sizes,
343 CM2.5 correctly simulates the largest TCs over the western North Pacific, but the dramatically
344 smaller average TCs over the eastern North Pacific in observations is not well-captured in the
345 model, indicating further room for improvement, perhaps in future models with higher
346 resolution. In response to CO₂ doubling, the mean simulated TC size, as measured by R12 and
347 R15, increases significantly over the globe, and in each of the individual basins except for the
348 South Indian, indicating that the coverage of strong TC wind gust may become larger in a
349 warmed climate. The changes in global mean TC size for R12, R15 and R25 are 3.3 %, 2.4 %
350 and 4.4 %, respectively, with similar increases being found over most of the basins. The South
351 Indian Ocean has a significant TC size increase, but only for the R25 metric.

352 Heavy rainfall induced by TCs is another principal source of TC damage, and is projected to
353 increase with climate warming (Knutson et al. 2010; 2013). We examine the CO₂-induced
354 changes in the TC rainfall in the CM2.5 simulations. Figure 9 summarizes the changes, between
355 the control and 2×CO₂ simulations, of average TC-related rainfall rates using all the TC periods
356 in these experiments. The results show a significant increase in rainfall rate near TCs in response
357 to CO₂ doubling (significance assessed using a two-sided t-test, $p < 0.05$). The fractional increase
358 in rainfall rate near the storms is much higher than the fractional increase of climatological
359 rainfall over tropical oceans in general (+3.8% averaged over 30S-30N). The fractional change
360 near the storm features a maximum increase for a 200km averaging radius about the storm
361 center, and smaller increases at larger (e.g., 350 km, 450 km) or smaller (150 km) averaging radii
362 . Knutson et al. (2013) also showed that fractional increase of TC rainfall becomes larger for

smaller averaging radii; in their experiments, the increase continued down to an averaging radius of 50 km (see Fig. 11 in Knutson et al. 2013). The discrepancy between the Knutson et al. (2013) results and the CM2.5 results in Fig. 9 may result from the coarser model resolution used in our experiments (i.e., models with 18- and 9-km grids were used in Knutson et al. (2013) versus about 50 km for CM2.5).

The global mean changes of TC rainfall rates are 12.2%, 13.3%, 12.1% and 11.3%, for averaging radii of 150, 250, 350 and 450 km, respectively, (Fig. 9c) but the rates vary from the basin to basin. The fractional increases are larger in the North Hemisphere basins than in the Southern Hemisphere. If we assume that the moisture convergence from the larger scale environments dominates the moisture budget near the TC, the mean increase of TC rainfall rate follows roughly the changes expected based on increases in the environmental water holding capacity of the atmosphere (which increases at about 7% per 1°C SST warming) (see also Knutson et al. 2013). Based on an increase of tropical SST of about 2.1°C in the CM2.5 CO₂ doubling experiment, the fractional increase of the environmental low-level water vapor content is about 14.7%. The water vapor content increases for each basin are similar (dotted bars in Fig. 9c). While the percent increases of the estimated lower tropospheric water vapor content for the Northern Hemisphere basins are similar to the simulated fractional changes of TC rainfall, the simulated TC rainfall response in the Southern Hemisphere basins is much smaller (Fig. 9c). This result is reminiscent of the TC intensity response in the model, in which the increase of TC intensity in the Southern Hemisphere basins was smaller than in the North Hemisphere (Table 2). The result suggests that TC intensity changes may play an important role (along with environmental water vapor changes) in the response of TC rainfall rates to large-scale climate warming.

Figure 10 shows maps of raw differences and percentage changes in the TC occurrence, sustained wind speeds, and the annually accumulated power dissipation for each 5x5 degree grid box, comparing the CM2.5 control and 2xCO₂ simulations. A 9-point Gaussian smoothing filter was applied to the maps for display purposes and statistically significant changes at the regional scale are indicated by the contours in the right column panels. In this study, the power dissipation is calculated by integrating the power dissipation rate¹ ($\rho C_d V^3$) (Bister and Emanuel (1998)) over the circle area that has the radius of R12 from TC center. In the figure, the power dissipation is accumulated over each TC's occurrence time in each grid and over the entire year, and thus represents an annual measure of the potential destructiveness of TCs (Emanuel 2005). By definition, the power dissipation is amplified exponentially as the wind speeds of TCs increase. Thus the power dissipation may be significantly biased low in CM2.5 since the model cannot simulate very intense TCs (e.g., Fig. 7).

Consistent with the reductions in the TC formations and lifetimes in the warm climate, a large substantial decrease is seen in the TC occurrence days over the global tropics and subtropics (Fig. 10a and d). The largest absolute decreases are simulated over the western North Pacific, extreme eastern North Pacific and in the southern Indian Ocean. This change is similar to the results of Zhao and Held (2012) or Murakami et al. (2012) that showed decreases of TC occurrence in the western part of the western North Pacific and an increase in the central Pacific in a warm-climate simulation (although using a different forcing scenario than the 2xCO₂ perturbation that we use). The percentage reduction of TC occurrence is most pronounced in the Atlantic, and Indian oceans and over the western most parts of the northern and southern Pacific

¹ ρ is the air density, C_d is the surface drag coefficient and V is the wind speed at low level. Here, we use the air density (ρ) of 1 kg m⁻³ and a drag coefficient (C_d) of 2×10^{-3} (Emanuel 1998).

basins. The regional changes are statistically significant mainly over the Indian Ocean and much of the western and northeast Pacific basins.

The average sustained TC wind speed shows an increase over most tropical storm regions except for the eastern part of the South Indian Ocean (Fig. 10 b, e). The percentage increase in TC wind speeds is most pronounced and statistically significant over a swath of the central Atlantic basin, over large parts of the three Pacific storm basins, and along the western edge of the Indian Ocean basin. The change is not statistically significant in the immediate vicinity of some key TC landfalling regions, including the Philippines, much of southeast Asia, and the eastern Gulf of Mexico/Florida/Caribbean region. A significant reduction is simulated in a small region near northwest Australia.

Although the TC occurrence and intensity have generally opposite directions of changes, the regional pattern of changes in power dissipation (Fig. 10c, f) tends to be more similar to those for TC occurrence than for intensity. The opposing changes in the accumulated power dissipation vs. TC intensity might occur because the changes in TC occurrence are larger in percentage terms than for TC wind speed. In fact, the power dissipation index (PDI) per TC (not annually accumulated) has a marginal increase (+3.4% for the globe) in response to CO₂ doubling (Table 2). However, the basin-wide annually accumulated power dissipation index change remains negative (-3.5 %) globally, due to the influence of reduced TC counts (Table 2).

An important question concerning TCs and climate change is whether the observed correlation between low-frequency variations of basin-wide Atlantic PDI and tropical Atlantic SST (Emanuel 2007) can be used to infer PDI changes due to radiatively forced climate change (e.g, Vecchi et al. 2008). The present results provide further support for the projection analysis of

Vecchi et al. (2008) that suggest that the Atlantic basin-wide PDI changes associated with global warming are not well described statistically by local tropical Atlantic SST changes alone.

The previous studies suggested that the “relative SST” over the Atlantic Main Development Region (MDR) have a strong statistical association with TC frequency in the NA basin (Zhao et al. 2009; Villarini et al. 2010, 2011; Vecchi et al. 2011). The relative SST here is defined as the SST over the MDR (SST_{MDR}) relative to the SST averaged over the global tropics. Using the statistical model developed by Villarini et al. (2011) for Atlantic TC counts, the relative SST changes simulated by CM2.5 imply a 10 % reduction in Atlantic TC count during August-October in response to the CO_2 doubling, which is a smaller decrease than obtained directly from the CM2.5 dynamical projection (-28 %). However, our results qualitatively supports the notion that relative SST is an important predictor variable for Atlantic TC frequency changes – even those in response to a CO_2 -induced global warming (Zhao et al. 2009, Knutson et al. 2013). It is notable that the some dynamical models do not project a reduction of Atlantic TCs in a climate warming scenario (e.g., Sugi et al. 2002, 2009; Emanuel et al. 2008; Oouch et al 2006). However, as shown in Villarini et al. (2011) and Knutson et al. (2013), models that project increased (decreased) Atlantic TC count usually have, or are being forced with, positive relative SST changes in the warmer climate.

Doi et al. (2013) found enhanced interannual variations of SST_{MDR} during early boreal summer in a CO_2 -warmed climate and suggested that the higher Atlantic TC counts could occur during warm SST_{MDR} years with the warmer climate than during warm SST_{MDR} years in the present climate, even if the mean Atlantic TC count were reduced overall. Because their TC inferences were derived from a statistical TC projection technique based on the relative SST, we re-examine this issue here based on the TC simulations in our dynamical model (CM2.5). Table 3a shows,

for both the control and 2xCO₂ climate, the mean Atlantic TC count for all years and the increases in the count during warm SST_{MDR} years. The warm SST_{MDR} years are defined as years when the SST_{MDR} is greater than one standard deviation over the climatological mean SST_{MDR} for either the control or 2xCO₂ runs. The results show that in the control simulation, Atlantic TC counts increase by 26% during warm SST_{MDR} years, while in the 2xCO₂ experiment the counts increase by 50% in warm SST_{MDR} years. Thus, despite the decrease in mean TC count in the Atlantic (-28%) in the 2xCO₂ run, the increase of TC counts during warm SST years is larger by 37% in 2xCO₂ run than in the control run.

A similar analysis is applied to annual PDI for Atlantic TCs yields similar results to the TC count (Table 3b). The deviation from the climatological mean of annual PDI for warm SST_{MDR} years is enhanced more than 200% in the 2xCO₂ run relative to the control run. The actual mean annual PDI for warm SST_{MDR} years also becomes larger in the 2xCO₂ run ($29.7 \times 10^3 \text{ m}^{-3} \text{ s}^{-3}$) than in the control run ($25.1 \times 10^3 \text{ m}^{-3} \text{ s}^{-3}$). These results must be viewed with caution due to the large negative biases in the genesis number and intensity of strong TCs in the Atlantic basin. Nevertheless, the results from CM2.5 for TC count and PDI support the findings of Doi et al. (2013) which were based on statistical downscaling only.

6. Summary and Discussion

In this study, we analyzed the TC activity simulated by the GFDL CM2.5 high-resolution coupled climate model. The CM2.5 model simulates globally aggregated TC activity fairly realistically, including the global TC frequency and seasonal cycle, although there are biases in regional TC activity. In the North Atlantic, too few TCs are simulated, which appears to be related to large-scale environmental biases in the simulation, including a cold bias in tropical

475 Atlantic SST, anomalous downward motion over much of the basin, and excessive vertical wind
476 shear in the model. Elsewhere in the tropics, TC simulation biases also appear to be related to
477 large-scale biases in the environmental fields. These results suggest a path for improving the
478 simulation skill for TC activity in the model by reducing the simulation biases in the large-scale
479 environment.

480 CM2.5 shows a notable ability to simulate the variability of TC activity related to ENSO.
481 Despite the biases in the regional climatological TC activity in CM2.5, a number of observed
482 ENSO-induced regional changes in TC activity over the globe are well captured by the model,
483 such as the eastward shift of TC occurrence over the Northwestern Pacific and reduced TC
484 occurrence over during the North Atlantic during El Nino. The encouraging simulation of the
485 ENSO-related TC activity changes suggests that the CM2.5 is a useful tool to explore the TC
486 response to the other large-scale environmental changes, such as those associated with global
487 warming. Moreover, because ENSO is one of the most important factors affecting regional TC
488 activity, CM2.5 is a good candidate model for developing long-term (seasonal to decadal)
489 prediction of the regional TC activity.

490 The response of TC activity in CM2.5 to global warming is evaluated here by comparing the
491 control run with a 2xCO₂ run. The results show a substantial reduction of global TC frequency (-
492 19%) in response to CO₂ doubling. The lifetime-maximum TC intensity increases by +2.7% in
493 response to CO₂ doubling. This pair of findings is consistent with most other current climate
494 modeling studies of TC behavior under climate warming (e.g., Knutson et al. 2010). However,
495 the TC intensity response of the model to CO₂ doubling should be viewed with caution, because
496 this model has a clear deficiency in simulating very strong TCs, due at least in part to its
497 resolution relative to hurricane scales. However, the results provide some further support for the

hypothesis that that frequency of the strongest TCs will increase in the 21st century due to climate warming, based on the shift of the intensity distribution toward higher maximum wind speeds in the 2xCO₂ run. The increase in frequency of strong TCs may be a more important factor for future TC damage potential than the decrease in total TC frequency, since a large fraction of historical TC damage has been caused by a relatively few strong TCs (Mendelsohn et al. 2012; Pielke et al. 2008). However, assessing the damage potential implied by the changes in various TC characteristics is beyond the scope of our study.

We have examined other factors known to contribute to TC damages such as lifetime, track length, translation speed, and storm size. TC damage tends to be larger when TC translation speed is slow (Mahendran 1998; Holland et al. 2010), and the TC size is large (Powell and Reinhold 2007, Maclay et al. 2008). In response to a CO₂ doubling, we find significant decreases in the average lifetime and track length but the translation speed has no significant changes. The TC size (horizontal extent of strong surface winds) shows some statistically significant increases (+2 to +4% depending on the size metric) in response to CO₂ doubling.

The TC rainfall rate, in response to CO₂ doubling, shows a significant increase over all basins, by about 8–18 % when averaged within a radius of 250 km from the TC center. This increase rate is broadly consistent with the previous studies (see Table S3 in Knutson et al. 2010). The percent increase in TC rainfall rate roughly scales with the increase in water holding capacity of the troposphere under 2xCO₂ (see also Knutson et al. 2013) at least over the northern hemisphere basins, although the increase is less than the simple scaling in the southern hemisphere basins. The smaller response in the southern hemisphere is probably related to the smaller intensification of TCs in the southern hemisphere basins than in the northern hemisphere.

520 We interpret the results as suggestive of a role for TC intensification in modulating the TC
521 rainfall response to global warming.

522 The responses of various TC characteristics to CO₂ doubling have a spatially inhomogeneous
523 regional structure. In general, the TC occurrence and intensity tend to exhibit regional changes
524 of opposite sign. That is, the two parameters have opposing tendencies but similar spatial
525 patterns of response to CO₂ doubling. The annual power dissipation response pattern tends to
526 follow more closely the TC occurrence response pattern due to larger proportional change of TC
527 occurrence compared to intensity.

528 The TC response to CO₂ doubling can be interpreted in terms of changes in environmental
529 parameters. In response to CO₂ doubling, the simulated changes in SST and static stability have
530 the same sign of change over the tropical region so they are good candidates to explain the
531 relatively spatially homogenous changes in TC activity (figure not shown). On the other hand,
532 the responses of vertical motion, relative humidity and vertical wind shear to CO₂ doubling
533 show more complicated spatial structure in their change fields. We speculate that these factors
534 are more responsible for modulating the models response of TC activity to the CO₂ doubling at
535 the regional (sub-basin) scale. However, we could not find significant relationship between any
536 single environmental parameter and TC response, suggesting the TC changes is not simple
537 response of a certain environmental factors.

538 The decrease (-28%) in TC frequency simulated for the Atlantic basin under 2xCO₂ is in
539 qualitative agreement with the decrease (-10%) obtained using a statistical projection of relative
540 MDR SST, which provides further support for the relative SST paradigm as a way of
541 synthesizing and understanding differences between Atlantic basin TC projections from different
542 studies and models.

We also find the fractional increase in TC count and PDI during anomalous warm years is greater in the 2xCO₂ climate than in the control climate. In other words, even though the climatological average PDI decreases in the 2xCO₂ climate, the PDI increases so much during anomalously warm individual years that those highly active years are more active than the most active years in the control climate. This supports the suggestion by Doi et al. (2013) that despite the reduced TC count in the Atlantic basin under 2xCO₂ conditions, the overall damage potential (aside from development and mitigation issues) may be elevated, although the topic needs further study to include other possible influences even from the climate perspective, such as sea level rise and landfalling activity.

The CM2.5 experiments are distinct from experiments using an atmospheric GCM running over prescribed SSTs because CM2.5 can simulate the atmosphere-ocean coupling processes. These processes are very important in TC development (e.g., Schade and Emanuel 1999; Bender and Ginis 2000), as well as in simulating the large-scale atmosphere-ocean circulations (e.g., Waliser et al. 1999; Douvill 2004). Therefore, the question arises as to the influence of ocean coupling on the response of TC activity to global warming. One of important process involving atmosphere-ocean interactions and TCs is the impact of the SST “cold wake” generated by the storm itself. In that regard, ocean coupling was assessed by Knutson et al. (2000) to have only a minor effect on the percent increase of TC intensity under climate warming. The effect of ocean coupling is examined in a different context in this study, as the ocean interacts with the changes in the atmosphere above it at all scales from the both the storm scale to the planetary scale. The storm scale interaction is probably limited by the coarse grid and weaker than observed TCs in the model, but the large-scale interaction adds an additional degree of realism beyond what one can obtain from the prescribed SST approach. Through the inclusion of more important

566 processes in TC-climate change simulations, we are striving for a better understanding of this
567 complex set of geophysical problems.

568

569

570 **References**

571 Bengtsson, L., M. Botzet, and M. Esch, 1996: Will greenhouse gas-induced warming over the
572 next 50 years lead to higher frequency and greater intensity of hurricanes? *Tellus A*, **48**, 57–
573 73, doi:10.1034/j.1600-0870.1996.00004.x.

574 Bengtsson, L., K. I. Hodges, M. Esch, N. Keenlyside, I. Kornbluh, J.-J. Luo, and T. Yamagata,
575 2007: How may tropical cyclones change in a warmer climate? *Tellus A*, **59**, 539–561,
576 doi:10.1111/j.1600-0870.2007.00251.x.

577 Bender, M. A., and I. Ginis, 2000: Real-case simulations of hurricane–ocean interaction using a
578 high-resolution coupled model: Effects on hurricane intensity. *Mon. Wea. Rev.*, **128**, 917–
579 946.

580 Bender, M. A., T. R. Knutson, R. E. Tuleya, J. J. Sirutis, G. A. Vecchi, S. T. Garner, and I. M. Held,
581 2010: Modeled impact of anthropogenic warming on the frequency of intense Atlantic
582 hurricanes. *Science*, **327**(5964), DOI:10.1126/science.1180568.

583 Broccoli, A. J., and S. Manabe, 1990: Can existing climate models be used to study
584 anthropogenic changes in tropical cyclone climate? *Geophys. Res. Lett.*, **17**, 1917–1920,
585 doi:10.1029/GL017i011p01917.

586 Camargo, S.J. and A.H. Sobel, 2005. Western North Pacific tropical cyclone intensity and
587 ENSO. *Journal of Climate*, **18**, 2996–3006.

588 Chu, P.-S. 2002: Large-scale circulation features associated with decadal variations of tropical
589 cyclone activity over the central North Pacific. *J. Climate*, **15**, 2678–2689.

590 Delworth, T. L. and Coauthors, 2006: GFDL’s CM2 Global Coupled Climate Models. Part I:
591 Formulation and Simulation Characteristics. *J. Climate*, **19**, 643–674,
592 doi:10.1175/JCLI3629.1.

593 Delworth, T. L. and Coauthors, 2011: Simulated Climate and Climate Change in the GFDL
594 CM2.5 High-Resolution Coupled Climate Model. *J. Climate*, **25**, 2755–2781,
595 doi:10.1175/JCLI-D-11-00316.1.

596 Doi, T., G. A. Vecchi, A. J. Rosati, and T. L. Delworth, 2012: Biases in the Atlantic ITCZ in
 597 Seasonal–Interannual Variations for a Coarse- and a High-Resolution Coupled Climate
 598 Model. *Journal of Climate*, **25**, 5494–5511, doi:10.1175/JCLI-D-11-00360.1.

599 Doi, T., G. A. Vecchi, A. J. Rosati, and T. L. Delworth, 2013: Response to CO2 doubling of the
 600 Atlantic Hurricane Main Development Region in a High-Resolution Climate Model.
 601 *Journal of Climate*, In press, doi:10.1175/JCLI-D-12-00110.1.

602 Emanuel, K. A. The dependence of hurricane intensity on climate. *Nature* **326**, 483–485 (1987).

603 Emanuel, K., 2007: Environmental factors affecting tropical cyclone power dissipation. *J.*
 604 *Climate*, **20**, 5497–5509.

605 Emanuel, K., R. Sundararajan, and J. Williams, 2008: Hurricanes and Global Warming: Results
 606 from Downscaling IPCC AR4 Simulations. *Bull. Amer. Meteor. Soc.* **89**, 347–367,
 607 doi:10.1175/BAMS-89-3-347.

608 Evan, A. T., and S. J. Camargo 2011: A climatology of Arabian Sea cyclonic storms, *J. Climate*,
 609 **24**, 140-158.

610 Goldenberg, S. B., and L. J. Shapiro, 1996: Physical Mechanisms for the Association of El Niño
 611 and West African Rainfall with Atlantic Major Hurricane Activity. *J. Climate*, **9**, 1169–
 612 1187.

613 Gualdi, S., E. Scoccimarro, and A. Navarra, 2008: Changes in Tropical Cyclone Activity due to
 614 Global Warming: Results from a High-Resolution Coupled General Circulation Model. *J.*
 615 *Climate*, **21**, 5204–5228, doi:10.1175/2008JCLI1921.1.

616 Griffies, S. M., 2010: Elements of MOM4P1. GFDL Ocean Group Tech. Rep. 6,
 617 NOAA/Geophysical Fluid Dynamics Laboratory, 444 pp. [Available online at
 618 <http://www.gfdl.noaa.gov/fms/>]

619 Haarsms, R. J., J. F. B. Mitchell and C. A. Senior, 1993; Tropical disturbances in a
 620 GCM. *Climate Dyn.*, **8**; 247-257.

621 Held, I. M., and M. Zhao, 2011: The Response of Tropical Cyclone Statistics to an Increase in
622 CO₂ with Fixed Sea Surface Temperatures. *J. Climate*, **24**, 5353–5364.

623 Hill, K. A., and G. M. Lackmann, 2009: Influence of Environmental Humidity on Tropical
624 Cyclone Size. *Monthly Weather Review*, **137**, 3294–3315, doi:10.1175/2009MWR2679.1.

625 Hill, K. A. and G. M. Lackmann, 2011: The Impact of Future Climate Change on TC Intensity
626 and Structure: A Downscaling Approach. *J. Climate*, **24**, 4644–4661. doi:
627 <http://dx.doi.org/10.1175/2011JCLI3761.1>

628 Holland, G. J., J. Done, C. Bruyere, C. Cooper, A. SuzukiParker, 2010: Model investigations of
629 the effects of climate variability and change on future Gulf of Mexico tropical cyclone
630 activity. *OTC Metocean 2010*, 20690, doi:10.4043/20690-MS

631 Jiang, H., Halverson, J.B., Zipser, E.J., 2008. Influence of environmental moisture on TRMM-
632 derived tropical cyclone precipitation over land and ocean. *Geophys. Res. Lett.* **35**(17),
633 L17806.

634 Kanamitsu, M., W. Ebisuzaki, J. Woollen, S.-K. Yang, J. J. Hnilo, M. Fiorino, and G. L. Potter,
635 2002: NCEP–DOE AMIP-II Reanalysis (R-2). *Bulletin of the American Meteorological*
636 *Society*, **83**, 1631–1643, doi:10.1175/BAMS-83-11-1631.

637 Kim, J.-H., S. J. Brown, R. E. McDonald, 2011: Future changes in tropical cyclone genesis in
638 fully dynamic ocean- and mixed layer ocean-coupled climate models: A low-resolution
639 model study. *Climate Dyn.*, **37**(3), 737–758, doi:10.1007/s00382-010-0855-6.

640 Klotzbach, P. J., 2011: The Influence of El Niño–Southern Oscillation and the Atlantic
641 Multidecadal Oscillation on Caribbean Tropical Cyclone Activity. *J. Climate*, **24**, 721–731.

642 Knapp, K. R., M. C. Kruk, D. H. Levinson, H. J. Diamond, and C. J. Neumann, 2010: The
643 International Best Track Archive for Climate Stewardship (IBTrACS). *Bull. Amer. Meteor.*
644 *Soc.*, **91**, 363–376.

645 Knutson, T. R., R. E. Tuleya, and Y. Kurihara, 1998: Simulated increase of hurricane intensities
646 in a CO₂-warmed climate. *Science*, **279**(5353), 1018–1020.

647 Knutson, T. R., R. E. Tuleya, W. Shen, and I. Ginis, 2001: Impact of CO₂-induced warming on
648 hurricane intensities simulated in a hurricane model with ocean coupling. *J. Climate*, **14**(11),
649 2458–2468.

650 Knutson, T. R., and Coauthors, 2010: Tropical cyclones and climate change. *Nature Geosci.*, **3**,
651 157–163.

652 Knutson, T. R., and Coauthors, 2013: Dynamical downscaling projections of 21st century
653 Atlantic hurricane activity: CMIP3 and CMIP5 Model-based scenarios, *J. Climate*,
654 Acceped.

655 Kuleshov, Y., L. Qi, R. Fawcett, and D. Jones, 2008: On tropical cyclone activity in the Southern
656 Hemisphere: Trends and the ENSO connection. *Geophys. Res. Lett.*, **35**, L14S08,
657 doi:10.1029/2007GL032983.

658 Landsea, C.W., G.D. Bell, W.M. Gray , and S.B. Goldenberg, 1998: The Extremely Active 1995
659 Atlantic Hurricane Season: Environmental Conditions and Verification of Seasonal
660 Forecasts, *Mon. Wea. Rev.* **126**, 1174–1193.

661 Lin, S.-J., 2004: A “vertically Lagrangian” finite-volume dynamical core for global models.
662 *Mon. Wea. Rev.*, **132**, 2293–2307

663 Lock, A. P., A. R. Brown, M. R. Bush, G. M. Martin, and R. N. B. Smith, 2000: A new boundary
664 layer mixing scheme. Part I: Scheme description and single-column model tests. *Mon. Wea.*
665 *Rev.*, **128**, 3187–3199

666 Maclay, K. S., M. DeMaria, and T. H. Vonder Haar, 2008: Tropical Cyclone Inner-Core Kinetic
667 Energy Evolution. *Mon. Wea. Rev.*, **136**, 4882–4898, doi:10.1175/2008MWR2268.1.

668 Mahendran, M., 1998: Cyclone Intensity Categories. *Wea. Forecasting*, **13**, 878–883.

669 Mendelsohn, R., K. Emanuel, S. Chonabayashi, and L. Bakkensen, 2012: The impact of climate
670 change on global tropical cyclone damage. *Nature Climate Change*, **2**, 205–209.

671 Murakami, H., and B. Wang, 2010: Future Change of North Atlantic Tropical Cyclone Tracks:
672 Projection by a 20-km-Mesh Global Atmospheric Model. *J. Climate*, **23**, 2699–2721,
673 doi:10.1175/2010jcli3338.1.

674 Moorthi, S., and M. J. Suarez, 1992: Relaxed Arakawa–Schubert: A parameterization of moist
675 convection for general circulation models. *Mon. Wea. Rev.*, **120**, 978–1002.

676 Murakami, H., B. Wang, and A. Kitoh, 2011: Future Change of Western North Pacific
677 Typhoons: Projections by a 20-km-Mesh Global Atmospheric Model. *J. Climate*, **24**, 1154–
678 1169, doi:10.1175/2010JCLI3723.1.

679 Murakami, H. and Coauthors, 2012: Future Changes in Tropical Cyclone Activity Projected by
680 the New High-Resolution MRI-AGCM. *J. Climate*, **25**, 3237–3260, doi:10.1175/JCLI-D-
681 11-00415.1.

682 Oouchi, K., J. Yoshimura, H. Yoshimura, R. Mizuta, S. Kusunoki, and A. Noda, 2006: Tropical
683 cyclone climatology in a global-warming climate as simulated in a 20 km-mesh global
684 atmospheric model: Frequency and wind intensity analyses. *J. Meteorol. Soc. Japan*, **84**,
685 259–276, doi:10.2151/jmsj.84.259.

686 Putman, W. M., and S.-J. Lin, 2007: Finite-volume transport on various cubed-sphere grids. *J.*
687 *Comput. Phys.*, **227**, 55–78.

688 Philip J. K., 2011: El Niño–Southern Oscillation’s Impact on Atlantic Basin Hurricanes and U.S.
689 Landfalls. *J. Climate*, **24**, 1252–1263.

690 Pielke, R. A., J. Gratz, C.W. Landsea, D. Collins, M. A. Saunders, and R. Musulin, 2008:
691 Normalized hurricane damages in the United States: 1990–2005. *Nat. Hazards Rev.*, **9**, 29–
692 42.

693 Powell, M. D. and T. A. Reinhold, 2007: Tropical cyclone destructive potential by integrated
694 kinetic energy. *Bull. Amer. Meteor. Soc.*, **87**, 513–526.

695 Smith, T.M., R.W. Reynolds, Thomas C. Peterson, and Jay Lawrimore, 2008: Improvements to
696 NOAA's Historical Merged Land-Ocean Surface Temperature Analysis (1880-2006). *J.*
697 *Climate*, **21**, 2283–2296.

698 Sugi, M., H. Murakami, and J. Yoshimura, 2009: A reduction in global tropical cyclone frequency
699 due to global warming. *SOLA*, **5**, 164–167.

700 Royer, J.-F., F. Chauvin, B. Timbal, P. Araspin, and D. Grimal, 1998: A GCM study of impact
 701 of greenhouse gas increase on the frequency of occurrence of tropical cyclones. *Climate*
 702 *Dyn.*, **38**, 307–343

703 Schade, L. R., and K. A. Emanuel, 1999: The ocean's effect on the intensity of tropical cyclones:
 704 Results from a simple coupled atmosphere–ocean model. *J. Atmos. Sci.*, **56**, 642–65.

705 Vecchi, G. A., and B. J. Soden, 2007: Increased tropical Atlantic wind shear in model projections
 706 of global warming. *Geophys. Res. Lett.*, **34**, L08702.

707 Vecchi, G. A., M. Zhao, H. Wang, G. Villarini, A. Rosati, A. Kumar, I. M. Held, R. Gudgel,
 708 2011: Statistical–Dynamical Predictions of Seasonal North Atlantic Hurricane
 709 Activity. *Mon. Wea. Rev.*, **139**, 1070–1082.

710 Vecchi, G.A., S. Fueglistaler, I.M. Held, T.R. Knutson, M. Zhao, 2013: Impacts of Atmospheric
 711 Temperature Changes on Tropical Cyclone Activity. *J. Climate* (in press) doi:
 712 10.1175/JCLI-D-12-00503.1.

713 Villarini, G., G. A. Vecchi, J. A. Smith, 2010: Modeling the Dependence of Tropical Storm
 714 Counts in the North Atlantic Basin on Climate Indices. *Mon. Wea. Rev.*, **138**, 2681–2705.

715 Vallarini, G, G. A. Vecchi, T. R. Knutson, M. Zhao, and J. A. Smith, 2011: North Atlantic
 716 tropical storm frequency response to anthropogenic forcing: Projections and sources of
 717 uncertainty. *J. Climate*, **24**(13), 3224–3238.

718 Walsh, K. J. E., M. Fiorino, C. W. Landsea, and K. L. McInnes, 2007: Objectively Determined
 719 Resolution-Dependent Threshold Criteria for the Detection of Tropical Cyclones in Climate
 720 Models and Reanalyses. *J. Climate*, **20**, 2307–2314.

721 Wang, B., and J. C. L. Chan, 2002: How strong ENSO events affect tropical storm activity over
 722 the Western North Pacific. *J. Climate*, **15**, 1643–1658.

723 Wang, H., J.-K. E. Schemm, A. Kumar, W. Wang, L. Long, M. Chelliah, G. D. Bell, and P. Peng,
 724 2009: A Statistical Forecast Model for Atlantic Seasonal Hurricane Activity Based on the
 725 NCEP Dynamical Seasonal Forecast. *Journal of Climate*, **22**, 4481–4500.

726 Yu, J., Y. Wang, and K. Hamilton, 2010: Response of Tropical Cyclone Potential Intensity to a
 727 Global Warming Scenario in the IPCC AR4 CGCMs. *J. Climate*, **23**, 1354–1373,
 728 doi:10.1175/2009JCLI2843.1.

729 Yoshimura, J., M. Sugi and A. Noda, 2006: Influence of greenhouse warming on tropical cyclone
 730 frequency. *J. Meteor. Soc. Japan*, 84, 405–428

731 Zhao, M. and I. M. Held, 2012: TC-permitting GCM Simulations of Hurricane Frequency
 732 Response to Sea Surface Temperature Anomalies Projected for the Late 21st Century. *J.*
 733 *Climate*, **25**, 2995–3009.

734 Zhao, M., I. M. Held, S.-J. Lin, G. A. Vecchi, 2009: Simulations of Global Hurricane
 735 Climatology, Interannual Variability, and Response to Global Warming Using a 50-km
 736 Resolution GCM. *J. Climate*, **22**, 6653–6678.

737 Zhao, M., I. M. Held, and S.-J. Lin, 2012: Some Counterintuitive Dependencies of Tropical
 738 Cyclone Frequency on Parameters in a GCM. *J. Atmos. Sci.*, **69**, 2272–2283.

739
 740
 741

742 Table Captions

743 Table 1. Changes in the annual number of TCs that reach tropical-storm and hurricane intensity
744 thresholds in response to a CO₂ doubling in the CM2.5 model. Statistically significant
745 changes are denoted by an asterisk (*) for $p < 0.01$ and open circle (o) for $p < 0.05$.

746

747 Table 2. Percent changes in TC-related parameters: lifetime-maximum wind speed, lifetime,
748 track length, translation speed, power dissipation index (PDI) per TC; and annually accumulated
749 PDI. Statistically significant changes are denoted by an asterisk (*) for $p < 0.01$ and open circle (o)
750 for $p < 0.05$.

751

752 Table 3. Mean Atlantic (a) TC count and (b) annual power dissipation index (PDI) for all
753 years and the mean anomaly for unusually warm years in the Main Development Regions
754 (MDR), defined as years in which SST_{MDR} anomalies exceed one standard deviation relative to
755 the long-term Control or 2xCO₂ climatology.

756

757

Figure 1. Tropical cyclone tracks in (a) observations for 1981-2000 and (b) the CM2.5 Control simulation for years 110-140. Tropical storm and hurricane intensities are denoted by light and dark gray, respectively.

Figure 2. Observed (1981-2000) and simulated (CM2.5 control run) annual TC counts in each basin.

Figure 3. The annual cycle of monthly TC frequency in observations and the CM2.5 Control simulation.

Figure 4. Bias in the CM2.5-simulated SST (a, d), vertical wind shear between 200 hPa and 850 hPa (b, e), and omega at 500 hPa (c, f) compared to observations for boreal (a-c) and austral summer (d-f). The warm (cold) colors represent environments that are generally more (less) favorable for TC development in CM2.5 compared with the observations

Figure 5. Scatter plot of the vertical wind shear over the main developing region (MDR) vs. the number of tropical storms over the Atlantic basin during August–October. The observations (grey dots) are based on the IBTrACS and NCEP R2 datasets for 1979-2011. The CM2.5 simulation results are shown in black (control run) and red (2xCO₂ run). The mean value of each of the samples is marked by an open square.

Figure 6. TC occurrence days regressed on the NINO3.4 index in observations (a, c) and the CM2.5 simulation (b, d) for boreal summer (a, b) and austral summer (c, d).

781

782 Figure 7. Box-whisker plots for TC lifetime-maximum wind speed (left panels) and TC lifetime
783 (right panels) based on the CM2.5 control and 2xCO₂ experiments. The two plots in the upper
784 panels are for global TCs while the six plots for the individual basins are in the lower panels.
785 The boxes denote the lower and upper quartiles (25th and 75th percentiles), and the band near the
786 middle of the box is the median of the samples. The whiskers extended to 1st and 99th
787 percentiles and the dot indicates the mean of each sample. The significance of differences
788 between the control and 2xCO₂ sample means for each basin or the globe are assessed using
789 the Mann-Whitney U-test; Significant differences are denoted by the asterisks (*) for $p<0.01$ and
790 open circles (o) for $p<0.05$.

791

792 Figure 8. Mean TC size, defined as the radius of (a) 12 m/s (R12), (b) 15 m/s (R15)
793 and (c) 25 m/s (R25) azimuthally-averaged tangential winds in the control (open
794 bar) and 2xCO₂ (close bar) simulations for each basin. The observational climatology of
795 R12 (Chavas and Emanuel 2010: CE10) for all basins and R15 and R25 (WG88) for the
796 Northwest Pacific (WP) basin are plotted as dashed bars. Significant differences between the
797 mean TC sizes in the Control and 2xCO₂ experiments are denoted by asterisks (*) for $p<0.01$
798 and open circles (o) for $p<0.05$ based on two-sided t-tests.

799

800 Figure 9. (a) Composite difference and (b) fractional change of TC rainfall rates over the
801 northern hemisphere between the control and CO₂ doubling experiments. (c) The fractional
802 change of rainfall rate averaged within 150km, 250km, 350km and 450km of the TC center for
803 the globe and each basin. The error bars denote the 90% confidence intervals and show that all
804 2xCO₂ – Control differences are statistically significant. The dotted lines represent the

805 approximate changes of the water holding capacity for each basin, (estimated as 7% per degree C
806 increase of basin-averaged SST).

807

808 Figure 10. Differences and percentage change between the CM2.5 control and 2×CO₂
809 simulations in the annual TC occurrence days (a, d); surface wind speed averaged across all TC
810 occurrences (b, e), and annual accumulated power dissipation (c, f) in each 5°×5° grid box. A
811 Gaussian smoothing filter was applied to the gridded values before plotting. Dark contours in
812 right panels denote statistical significance at the $p < 0.05$ level.

813

814

Table 1. Changes in the annual number of TCs that reach tropical-storm and hurricane intensity thresholds in response to a CO2 doubling in the CM2.5 model. Statistically significant changes are denoted by an asterisk (*) for $p<0.01$ and open circle (o) for $p<0.05$.

	> Tropical Storms			> Hurricanes			Ratio	
	(A)			(B)			(B/Ax100)	
	Control	2xCO2	Percent Change	Control	2xCO2	Percent Change	Control	2xCO2
	(yr ⁻¹)	(yr ⁻¹)	(%)	(yr ⁻¹)	(yr ⁻¹)	(%)	(%)	(%)
Global	82.0	66.6	-18.8*	31.6	28.7	-9.2°	38.5	43.1
NA	2.7	1.9	-27.6*	0.4	0.3	-25.0	14.8	15.8
EP	16.6	13.9	-16.3*	3.0	3.5	16.7	18.1	25.2
WP	27.5	23.1	-16.0*	14.4	13.3	-7.6	52.4	57.6
NI	5.5	4.8	-12.7°	2.0	2.0	0.0	36.4	41.7
SI	21.7	16.5	-24.0*	8.8	6.8	-22.7*	40.6	41.2
SP	7.8	6.3	-19.2°	3.1	2.6	-16.1	39.7	41.3

Table 2. Percent changes in TC-related parameters: lifetime-maximum wind speed, lifetime, track length, translation speed, power dissipation index (PDI) per TC; and annually accumulated PDI. Statistically significant changes are denoted by an asterisk (*) for $p < 0.01$ and open circle (o) for $p < 0.05$.

	Global	NA	EP	WP	NI	SP	SI
Maximum Wind Speed	* 2.7%	° 4.3%	*4.6%	*2.5%	° 3.2%	2.0%	1.5%
Lifetime	*-4.6%	-2.0%	-0.6%	*-5.8%	-3.6%	-4.4%	*-7.8%
Travel Distance	*-4.0%	-1.7%	0.6%	°-5.0%	-1.8%	-4.0%	*-10.5%
Translation Speed	0.6%	2.7%	0.9%	1.7%	°6.9%	-0.8%	°-3.0%
PDI	° 3.4%	12.7%	*12.0%	3.1%	5.0%	2.3%	-3.8%
Annually Accumulated PDI	-3.5%	-10.7%	-7.1%	-4.6%	3.4%	-7.6%	°-11.9%

Table 3. Mean Atlantic (a) TC count and (b) annual power dissipation index (PDI) for all years and the mean anomaly for unusually warm years in the Main Development Regions (MDR), defined as years in which SST_{MDR} anomalies exceed one standard deviation relative to the long-term Control or 2xCO₂ climatology.

(a)	Mean TC count (A)	Anomalous TC count for warm SST _{MDR} years (B)	Percentage change (B/Ax100)
Control	2.7	+0.7	+25.9%
2xCO ₂	1.9	+1.0	+49.7%
2xCO ₂ minus Control	-0.76 (-28.3%)	+0.3 (+37.1%)	

(b)	Mean PDI (C)	Anomalous PDI for warm SST _{MDR} years (D)	Percentage change (D/Cx100)
Control	4.9	+0.5	+10.4%
2xCO ₂	4.4	+2.0	+46.4%
2xCO ₂ minus Control	-0.5 (-10.6%)	+1.5 (+297.5%)	

PDI unit is 10⁸ m⁻³ s⁻²

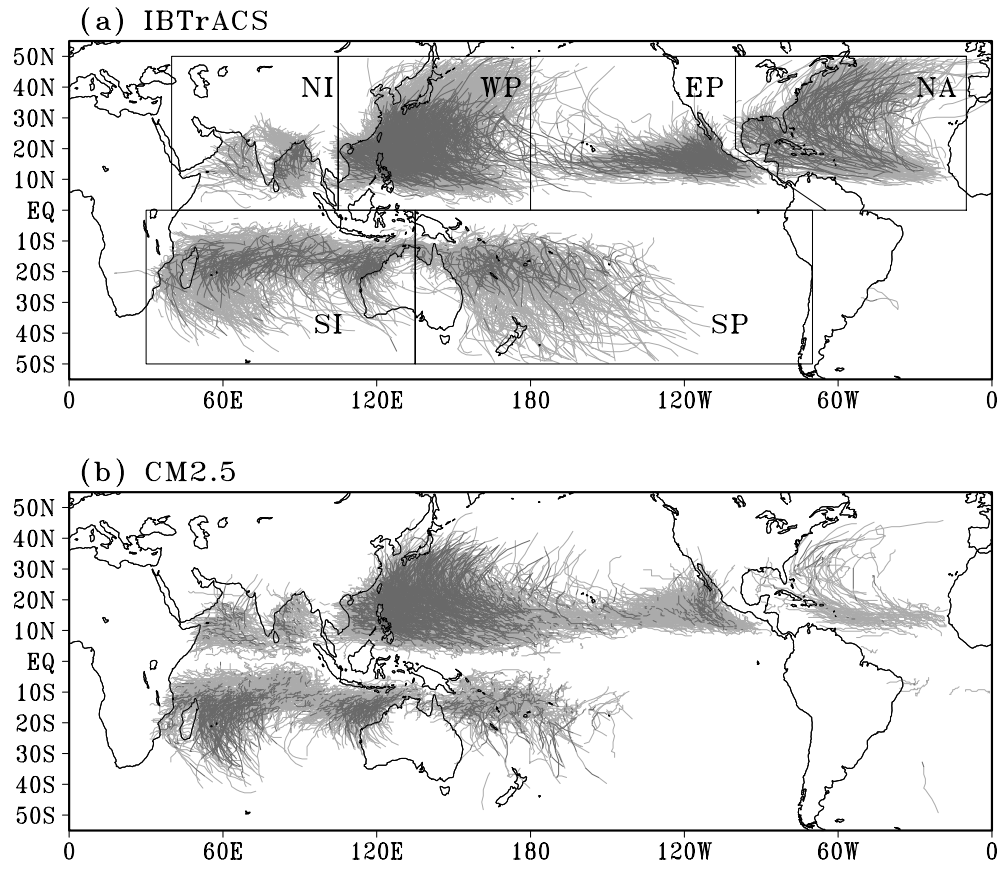


Figure 1. Tropical cyclone tracks in (a) observations for 1981-2010 and (b) the CM2.5 Control simulation for years 110-140. Tropical storm and hurricane intensities are denoted by light and dark gray, respectively.

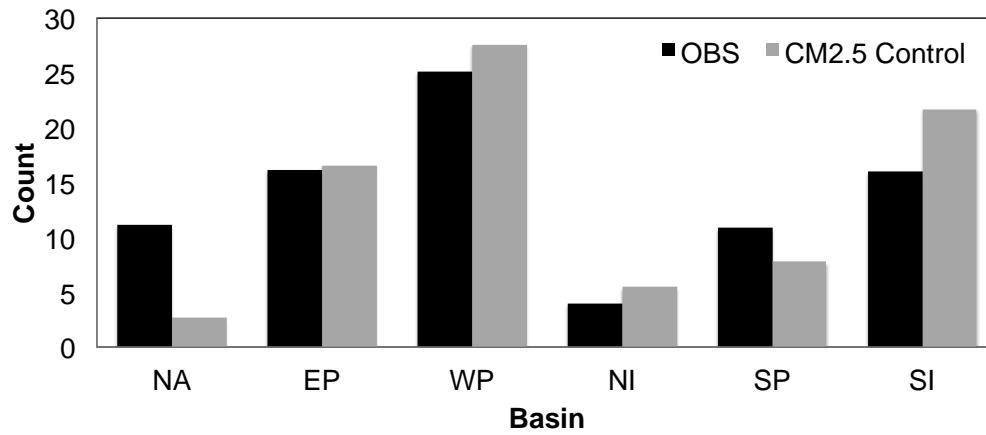


Figure 2. Observed (1981-2000) and simulated (CM2.5 control run) annual TC counts in each basin.

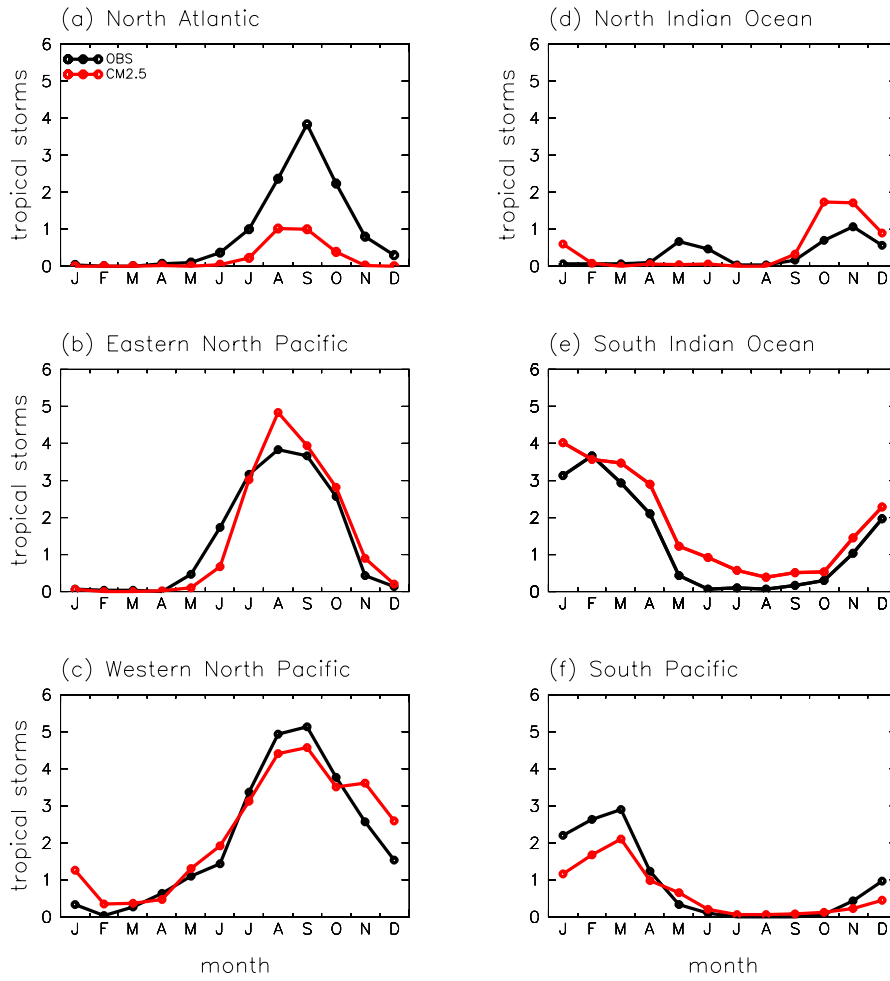


Figure 3. The annual cycle of monthly TC frequency in observations and the CM2.5 Control simulation.

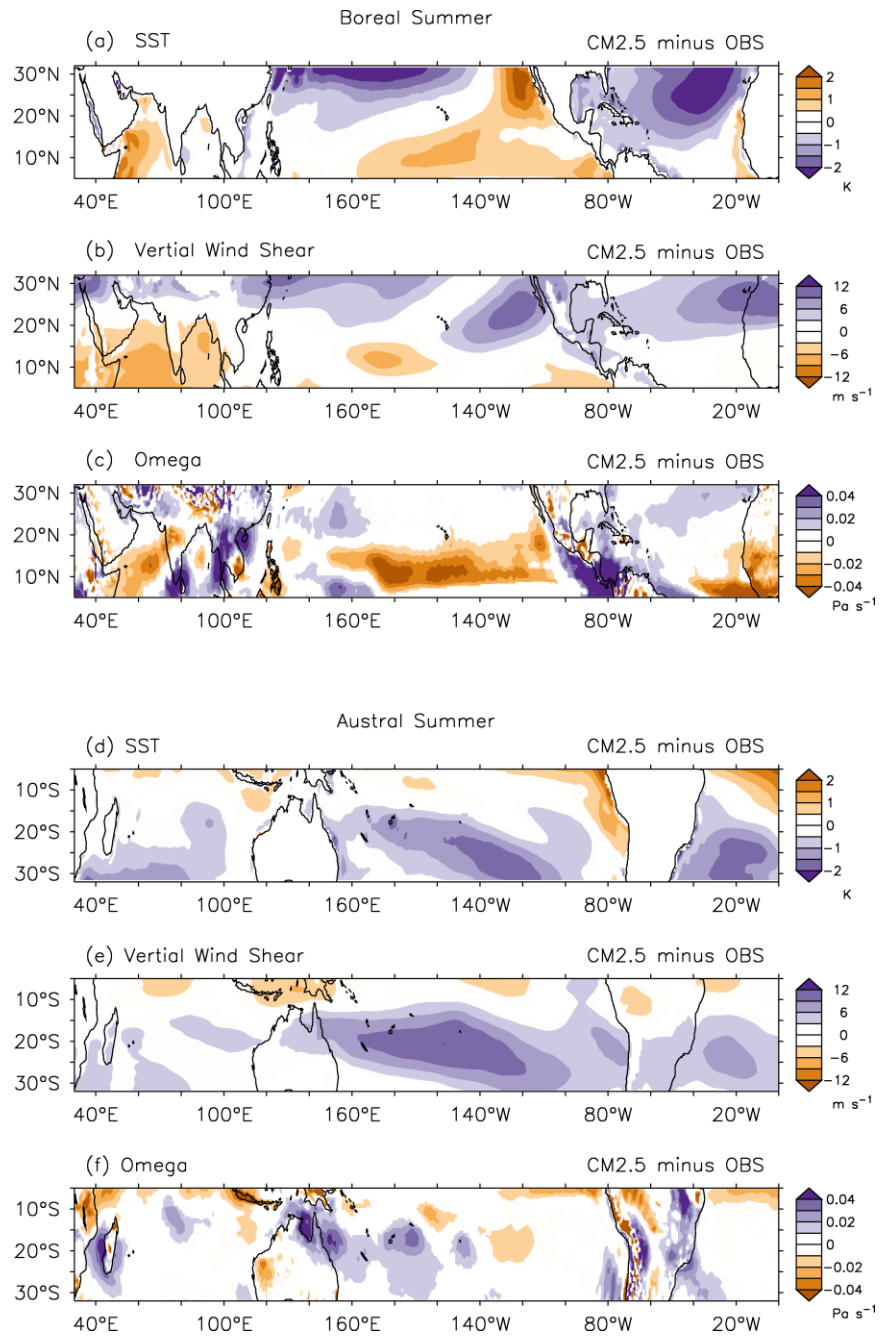


Figure 4. Bias in the CM2.5-simulated SST (a, d), vertical wind shear between 200 hPa and 850 hPa (b, e), and omega at 500 hPa (c, f) compared to observations for boreal (a-c)

and austral summer (d-f). The warm (cold) colors represent environments that are generally more (less) favorable for TC development in CM2.5 compared with the observations

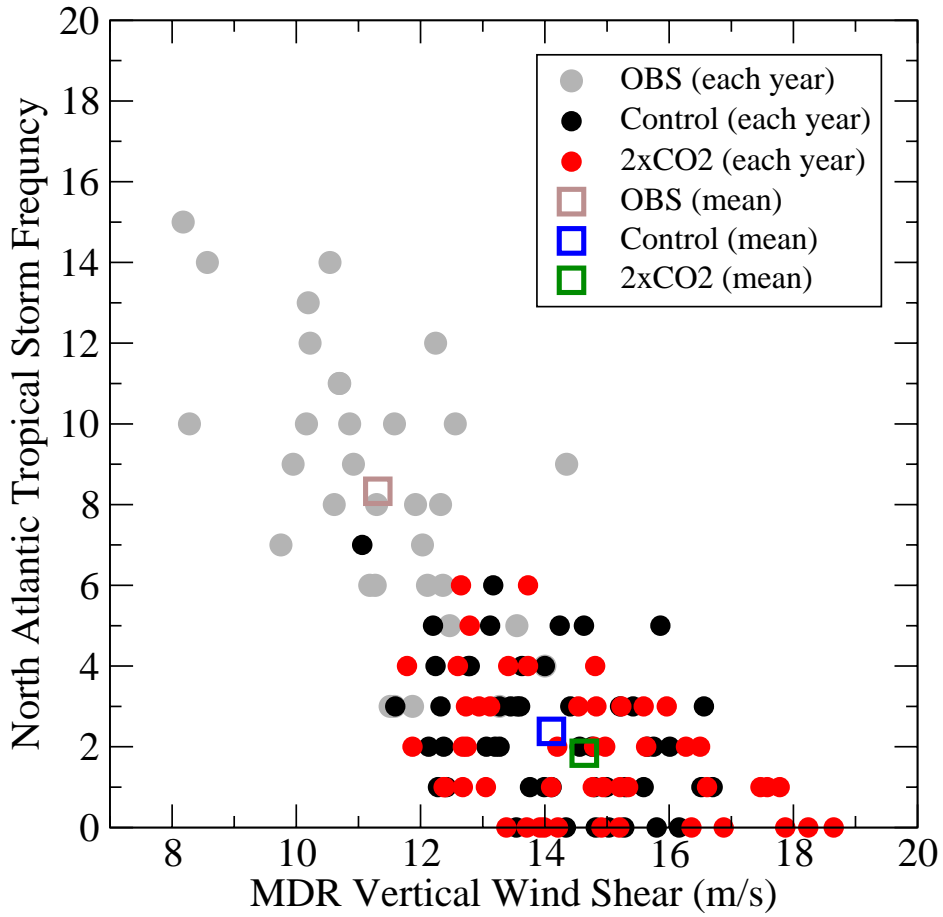


Figure 5. Scatter plot of the vertical wind shear over the main developing region (MDR) vs. the number of tropical storms over the Atlantic basin during August–October. The observations (grey dots) are based on the IBTrACS and NCEP R2 datasets for 1979–2011. The CM2.5 simulation results are shown in black (control run) and red (2xCO₂ run). The mean value of each of the samples is marked by an open square.

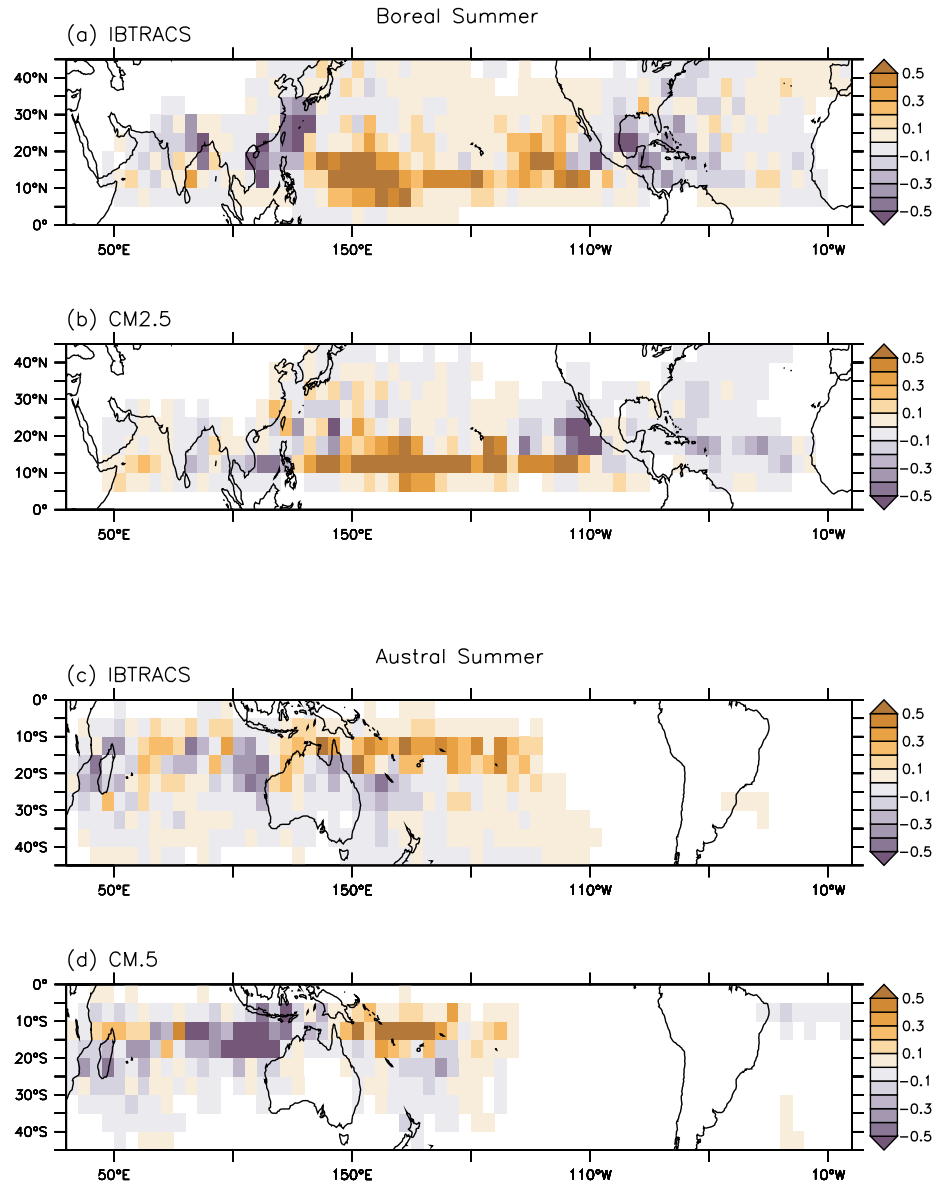


Figure 6. TC occurrence days regressed on the NINO3.4 index in observations (a, c) and the CM2.5 simulation (b, d) for boreal summer (a, b) and austral summer (c, d).

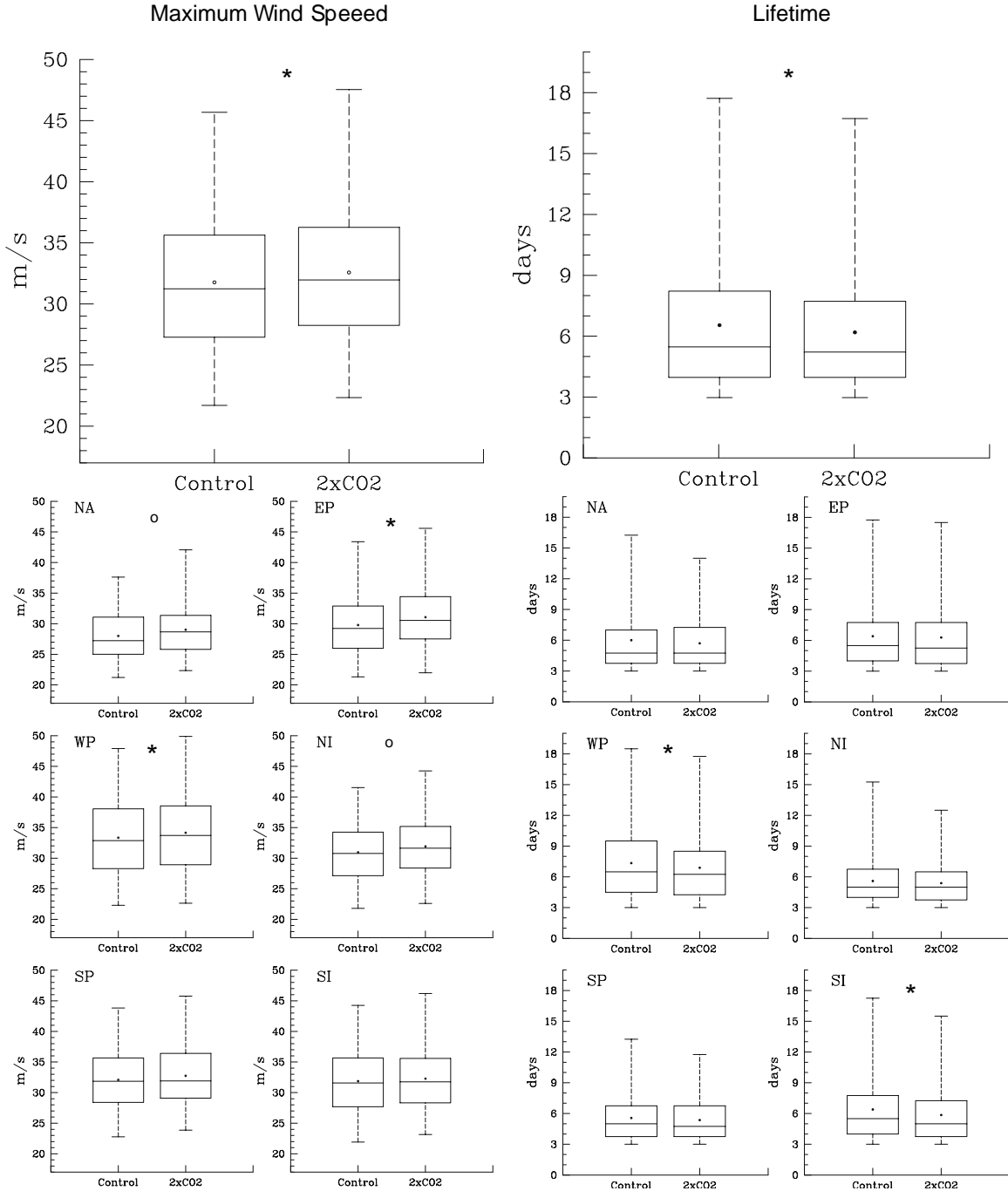


Figure 7. Box-whisker plots for TC lifetime-maximum wind speed (left panels) and TC lifetime (right panels) based on the CM2.5 control and 2xCO₂ experiments. The two plots in the upper panels are for global TCs while the six plots for the individual basins are in

the lower panels. The boxes denote the lower and upper quartiles (25th and 75th percentiles), and the band near the middle of the box is the median of the samples. The whiskers extended to 1st and 99th percentiles and the dot indicates the mean of each sample. The significance of differences between the control and 2xCO₂ sample means for each basin or the globe are assessed using the Mann-Whitney U-test; Significant differences are denoted by the asterisks (*) for $p < 0.01$ and open circles (o) for $p < 0.05$.

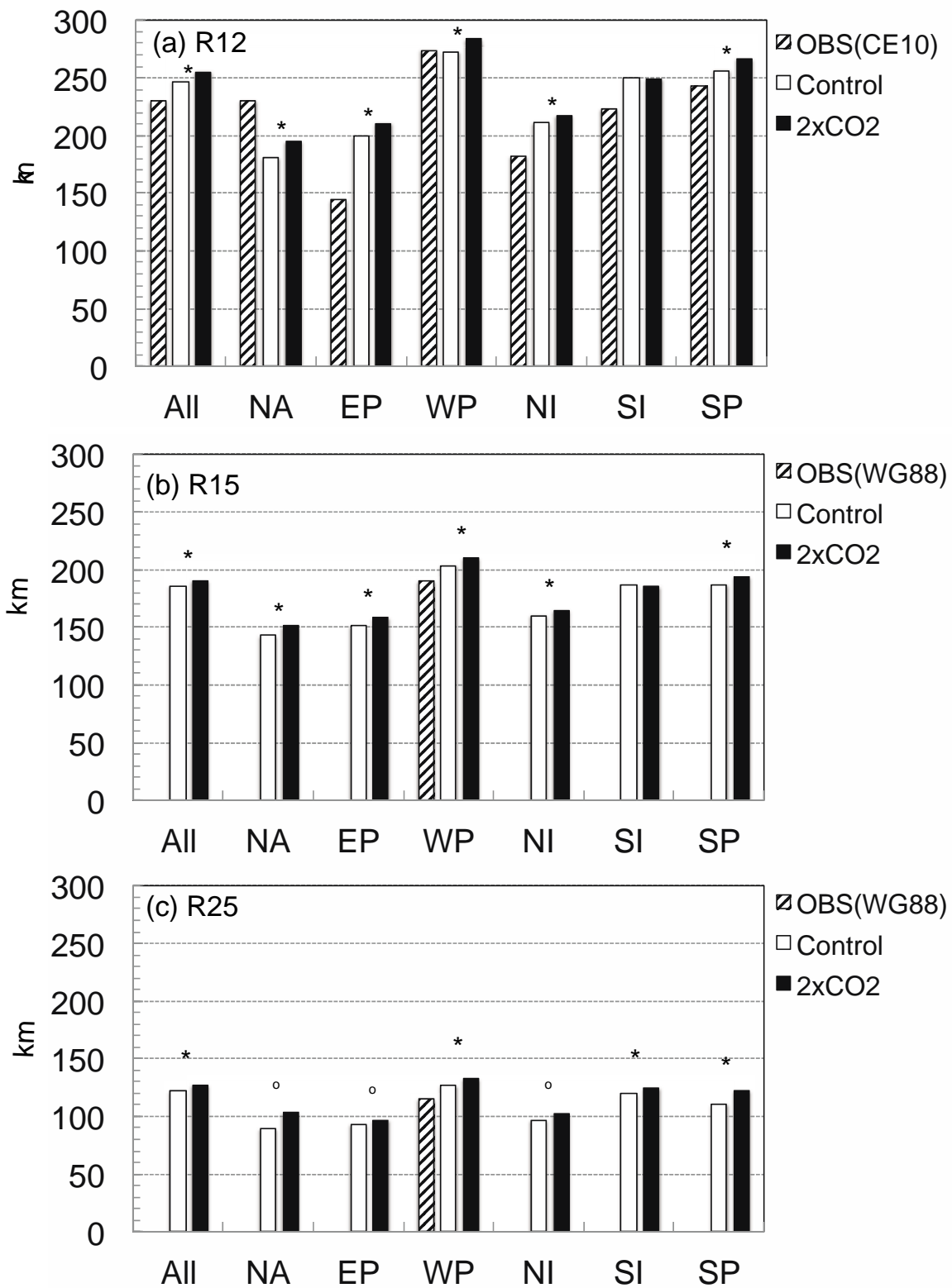


Figure 8. Mean TC size, defined as the radius of (a) 12 m/s (R12), (b) 15 m/s (R15)

and (c) 25 m/s (R25) azimuthally-averaged tangential winds in the control (open bar) and 2xCO₂ (close bar) simulations for each basin. The observational climatology of R12 (Chavas and Emanuel 2010: CE10) for all basins and R15 and R25 (Weatherford and Gray 1988: WG88) for the Northwest Pacific (WP) basin are plotted as dashed bars. Significant differences between the mean TC sizes in the Control and 2xCO₂ experiments are denoted by asterisks (*) for $p < 0.01$ and open circles (o) for $p < 0.05$ based on two-sided t-tests.

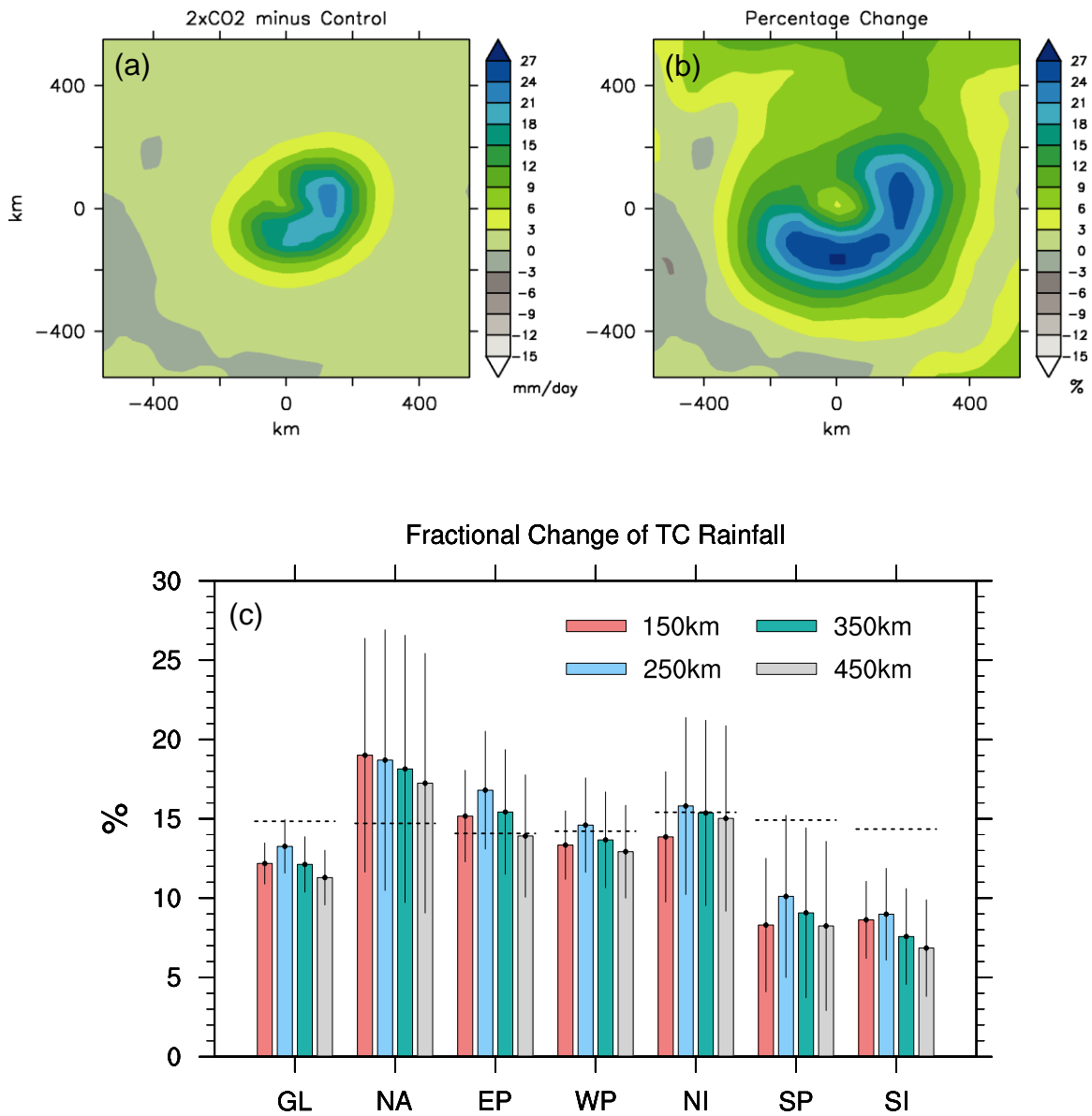


Figure 9. (a) Composite difference and (b) fractional change of TC rainfall rates over the northern hemisphere between the control and CO₂ doubling experiments. (c) The fractional change of rainfall rate averaged within 150km, 250km, 350km and 450km of the TC center for the globe and each basin. The error bars denote the 90% confidence intervals and show that all 2xCO₂ – Control differences are statistically significant. The dotted lines represent the approximate changes of the water holding capacity for each basin, (estimated as 7% per degree C increase of basin-averaged SST).

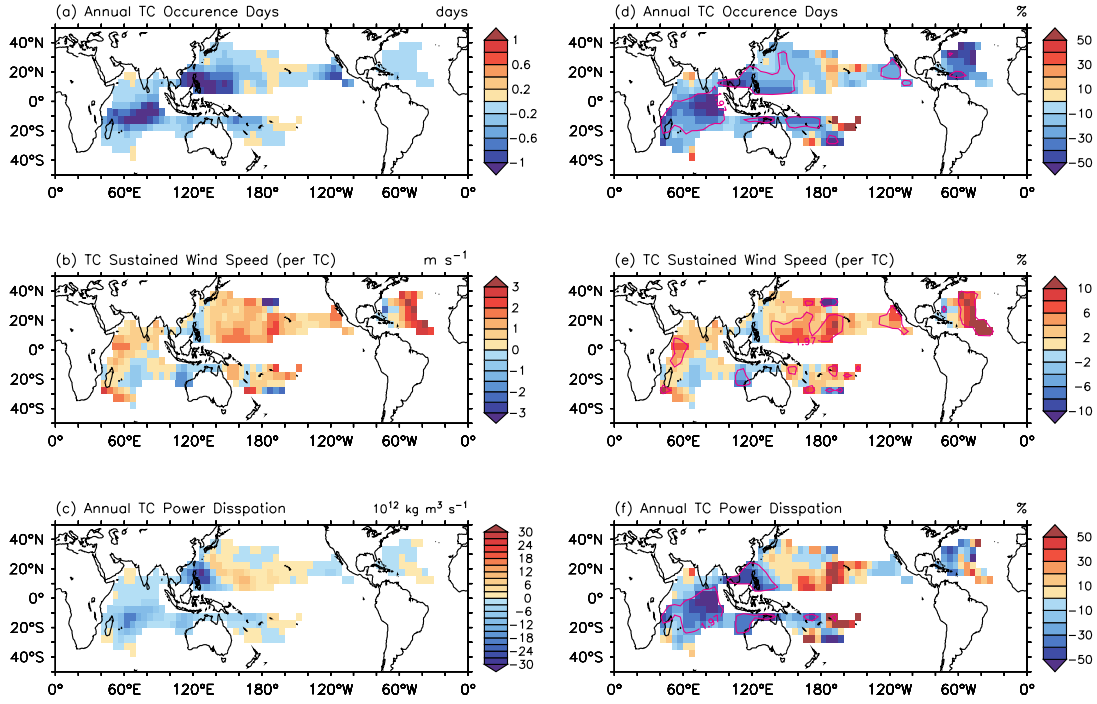


Figure 10. Differences and percentage change between the CM2.5 control and $2\times\text{CO}_2$ simulations in the annual TC occurrence days (a, d); surface wind speed averaged across all TC occurrences (b, e), and annual accumulated power dissipation (c, f) in each $5^\circ\times 5^\circ$ grid box. A Gaussian smoothing filter was applied to the gridded values before plotting. Dark contours in right panels denote statistical significance at the $p < 0.05$ level.